Site preference for Mn substitution in spintronic $CuM^{III}X_2^{VI}$ chalcopyrite semiconductors

Yu-Jun Zhao and Alex Zunger
National Renewable Energy Laboratory, Golden, Colorado 80401, USA
(Received 22 August 2003; revised manuscript received 10 October 2003; published 19 February 2004)

The quest for combining semiconducting with ferromagnetic properties has recently led to the exploration of Mn substitutions not only in *binary* (GaAs, CdTe), but also in *ternary* semiconductors such as chalcopyrites $AB^{III}X_2^{VI}$. Here, however, Mn would substitute any of the two metal sites *A* or *B*. The site preference of Mn doping in $CuM^{III}X_2^{VI}$ chalcopyrite is crucial because it releases different type of carriers: electrons for substitution on the Cu sites, and holes for substitution on the M^{III} sites. Using first-principles calculation we show that Mn prefers the M^{III} site under Cu-rich and III-poor conditions, and the Cu site under III-rich condition. We establish the chemical potential domains for pure $CuAlS_2$, $CuGaS_2$, $CuInS_2$, $CuGaSe_2$, and $CuGaTe_2$ stability. We show that the solubility of Mn on the M^{III} (Cu) site increases (decreases) as the Fermi level moves toward the conduction-band minimum (*n*-type conditions). It is further found that domains of chemical stability of all these chalcopyrites may be largely reduced by Mn incorporation.

DOI: 10.1103/PhysRevB.69.075208 PACS number(s): 75.50.Pp, 71.55.Ht

I. INTRODUCTION

The quest[1,2] for room-temperature ferromagnetic semiconductors that can be lattice matched to conventional compound semiconductors resulted in a recent interest in Mn doping of binary[1,3] (GaAs, GaN, GaP, InAs) as well as ternary[4–7] semiconductors. While in *binary* systems Mn substitution clearly occurs on the cation site, in *ternary* pnictides $A^{II}M^{IV}X_2^{V}$ (e.g., $ZnGeP_2$) or chalcopyrite $A^{I}M^{III}X_2^{VI}$ (e.g., $CuGaSe_2$) the site preference for Mn is unclear. Recent calculations for Mn in $CdGeP_2$ or $ZnGeP_2$ (Ref. 6,7) suggest that both cation site can be substituted, whereas calculations on Mn in $CuGaSe_2$ and $CuGaS_2$ considered substitution mostly on the M^{III} site.[5,8] The site preference is important since substitution on a lower valent site Mn_{Cu} is expected to be a donor (releasing electrons), whereas substitution on a higher valent site Mn_{III} is an acceptor (releasing holes). Only holes are expected to lead to ferromagnetism according to Dietl's work.[9] The present paper show how first-principles calculations can determine the site preference as a function of doping (Fermi energy) and the chemical potentials of Cu and M^{III}. We find that Mn prefers the M^{III} site under Cu-rich and III-poor conditions, whereas it prefers the Cu site under III-rich condition. As the Fermi level increases in the band gap, the solubility of Mn on the M^{III} site increases, while that on the Cu site decreases and disappears when E_F passes the mid-gap. When E_F is close to the valence-band maximum (VBM), the Mn_{III} is always charge neutral, while Mn_{Cu} is at $+1$ charge state. When E_F is located near the conduction band minimum (CBM), both Mn_{III} and Mn_{Cu} are in the negative charge state. Furthermore, the Mn chemical potential strongly affects the stability of the host materials: under extremely Mn-rich condition, the chalcopyrite host itself may discompose.

II. STABILITY OF PURE CHALCOPYRITE

The site preference of Mn depends on the formation energies for substitution, i.e. on $\Delta H_f(Mn_{Cu})$ and $\Delta H_f(Mn_{III})$, which are related to the allowed chemical potentials in the system. In this section we discuss the stability of pure chalcopyrite, I-III-VI_2, as exemplified by $CuAlS_2$.

First, to avoid precipitation of elemental solids, the atomic chemical potentials should be smaller than that of the corresponding elemental solid. Denoting $\Delta\mu_\alpha=\mu_\alpha-\mu_\alpha^{\text{solid}}$ we thus have

$$\Delta\mu_{\text{Cu}}\leqslant 0,\quad \Delta\mu_{\text{Al}}\leqslant 0,\quad \Delta\mu_{\text{S}}\leqslant 0, \tag{1}$$

Second, at equilibrium the sum of chemical potentials for all atoms must equal to the formation energy of the compound. Therefore

$$\Delta\mu_{\text{Cu}}+\Delta\mu_{\text{Al}}+2\Delta\mu_S=\Delta H_f(\text{CuAlS}_2), \tag{2}$$

where $\Delta\mu$ is the chemical potential relative to that of corresponding element solid. Equations (1) and (2) limit the chemical potentials in the triangle with vertexes decided by $(\Delta\mu_{\text{Cu}},\Delta\mu_{\text{Al}},\Delta\mu_{\text{S}})$. For visual simplicity, the triangle is projected to $(\Delta\mu_{\text{Cu}},\Delta\mu_{\text{Al}})$ space in Fig. 1. In this triangle, $A=(0,0)$ means Cu rich and Al rich; $B=[\Delta H_f(\text{CuAlS}_2),0]$ means Cu-poor and Al-rich; and $C=[0,\Delta H_f(\text{CuAlS}_2)]$ means Cu-rich and Al-poor. At point *A*, we have $\Delta\mu_{\text{S}}=\Delta H_f(\text{CuAlS}_2)/2$, i.e., S poor; points on the *BC* line mean $\Delta\mu_{\text{S}}=0$, i.e., S rich. Each line which is parallel to the *BC* line in the *ABC* triangle represents a constant $\Delta\mu_{\text{S}}$, decreasing from line *BC* to point *A*.

Third, the chemical potentials are further restricted by possible competing binary phases formed from the elemental constituents. This results in additional constraints:

$$\Delta\mu_{\text{Al}}+\Delta\mu_{\text{S}}\leqslant\Delta H_f(\text{AlS}), \tag{3}$$

$$2\Delta\mu_{\text{Al}}+3\Delta\mu_{\text{S}}\leqslant\Delta H_f(\text{Al}_2\text{S}_3), \tag{4}$$

$$\Delta\mu_{\text{Cu}}+\Delta\mu_{\text{S}}\leqslant\Delta H_f(\text{CuS}), \tag{5}$$

$$2\Delta\mu_{\text{Cu}}+\Delta\mu_{\text{S}}\leqslant\Delta H_f(\text{Cu}_2\text{S}), \tag{6}$$

$$\Delta\mu_{\text{Al}}+\Delta\mu_{\text{Cu}}\leqslant\Delta H_f(\text{AlCu}), \tag{7}$$

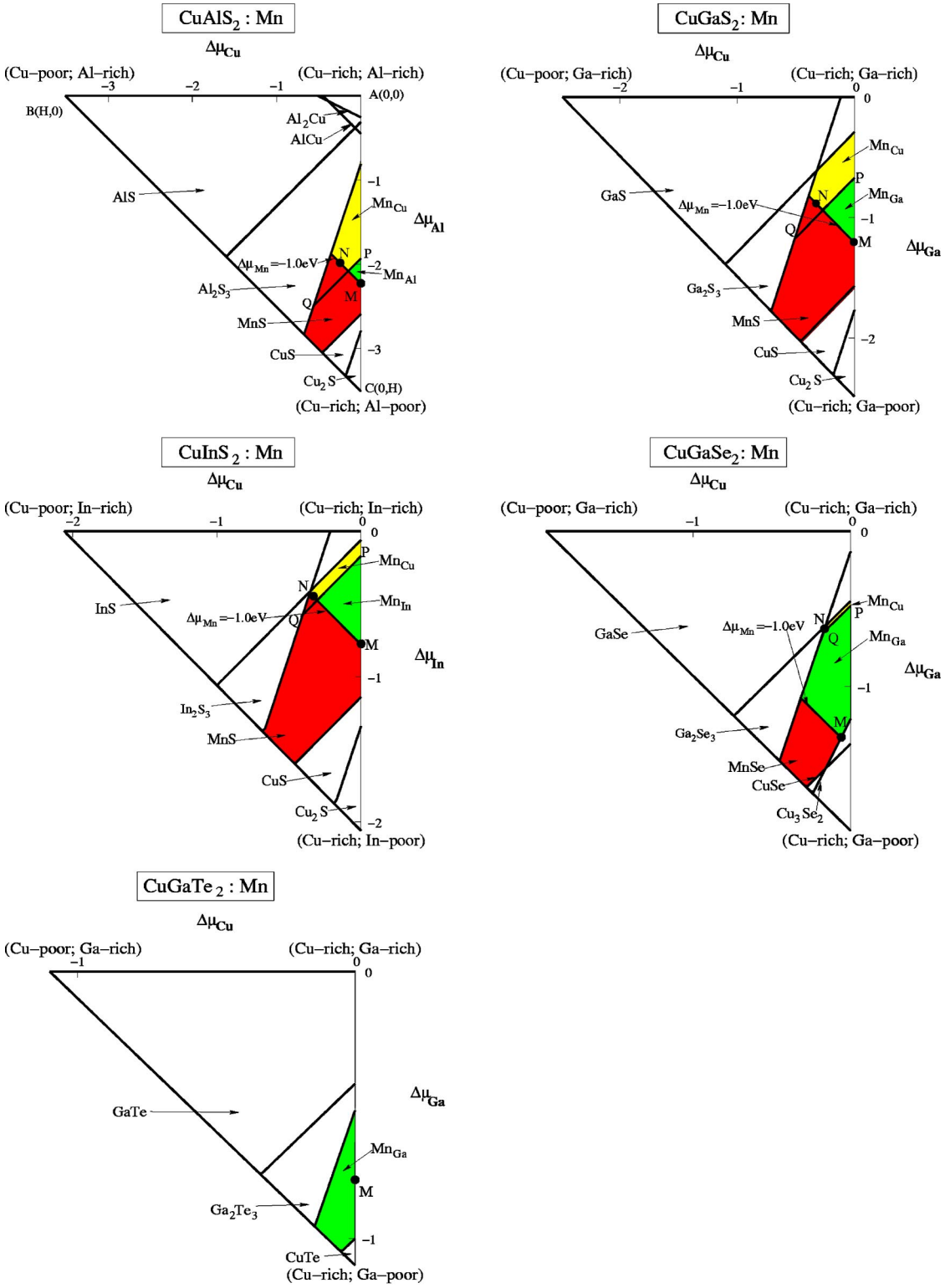

FIG. 1. (Color online). The density functional calculated allowed chemical potential ranges (sum of all the colored parts) for $CuAlS_2$, $CuGaS_2$, $CuInS_2$, $CuGaSe_2$, and $CuGaTe_2$. Yellow: Mn_{Cu} stable ($E_F = 0.1$ eV); Green: Mn_{III} stable ($E_F = 0.1$ eV); Red: decomposition into MnS, MnSe ($\Delta\mu_{Mn} = -1.0$ eV). The white regions are areas which are excluded due to the formation of competing phases specified in the figures (e.g., AlS, Al_2S_3). The allowed ranges may be decreased due to MnS or MnSe precipitates (red part in the figure assuming $\Delta\mu_{Mn} = -1.0$ eV); the chemical potential ranges for MnS or MnSe precipitates (red part) will be enlarged when $\Delta\mu_{Mn}$ increases (i.e., Mn gets richer). When E_F increases, the separating line PQ will shift up, i.e., chemical potential domain for Mn on III sites grows. For $CuGaTe_2$:Mn, there is no yellow region because the separating line PQ is in GaTe domain, and the red area will not appear until $\Delta\mu_{Mn}$ is greater than -0.61 eV.

TABLE I. Cohesive energies for the element solids, and formation energies of competing binary phases and of chalcopyrites. The experiment formation energies are from Ref. 24. The structures are taken from Ref. 25, except where other references are given.

Compound	Structure	Calculation (eV)	Expt (eV)
Mn	fcc AFM (Ref. 26)	3.26	2.98
Cu	cF4	3.55	3.50
Al	cF4	3.70	3.34
Ga	oC4	2.92	2.78
In	tI2	2.60	2.6
S	hP3	4.04	2.86
Se	hP3	3.51	2.13
Te	hP3	3.16	2.0
CuS	hP12	-0.46	
Cu_2S	tP12	-0.36	
CuSe	hP12	-0.28	
Cu_3Se_2	tP10	-0.72	
CuTe	oP4	-0.34	
Cu_2Te	oP6	0.11	
AlS	(GaS stru.)	-1.91	
GaS	hP8	-1.39	
InS	oP8	-1.06	
GaSe	hP8	-1.19	
GaTe	mC24	-1.05	
Al_2S_3	Defect zinc blende (Ref. 27)	-5.67	
Ga_2S_3	Defect zinc blende (Ref. 27)	-3.56	
In_2S_3	Defect zinc blende (Ref. 27)	-2.77	
Ga_2Se_3	Defect zinc blende (Ref. 28)	-2.96	
Ga_2Te_3	defect zinc-blende (Ref. 27)	-1.62	
MnS	NaCl structure (Ref. 29) AFM-II	-1.64	
MnSe	NaCl structure (Ref. 29) AFM-II	-1.27	
MnTe	NaCl structure (Ref. 29) AFM-I	-0.61	
AlCu	mC20	-0.45	
Al_2Cu	tI12	-0.51	~ -0.5 (Ref. 30)
Al_6Mn	oC28	-1.31	~ -1.3 (Ref. 30)
$CuAlS_2$	chalcopyrite	-3.51	
$CuGaS_2$	chalcopyrite	-2.49	
$CuInS_2$	chalcopyrite	-2.06	
$CuGaSe_2$	chalcopyrite	-1.93	-3.27 (Ref. 31)
$CuGaTe_2$	chalcopyrite	-1.10	

$$2\Delta\mu_{\mathrm{Al}}+\Delta\mu_{\mathrm{Cu}}\leqslant\Delta H_f(\mathrm{Al_2Cu}). \tag{8}$$

As shown in Fig. 1, $CuAlS_2$ is unstable with respect to formation of Al_2S_3 in the upper white area of Fig. 1, i.e., under Al-rich condition, (AlS, AlCu, and Al_2Cu pose weaker constrains, and are included in the Al_2S_3 ranges in Fig. 1). $CuAlS_2$ is also unstable with respect to CuS or Cu_2S precipitation in the lower white area, i.e., under Cu-rich and Al-poor condition. Thus, the total colored area (red + green + yellow) in Fig. 1 represents the chemical potential domain for which $CuAlS_2$ is stable.

In order to *quantitatively* evaluate the chemical potentials at which $CuM^{III}X_2^{VI}$ is stable with respect to competing phases, we need to know the elemental cohesive energies E_C [for Eq. (1)], as well as the compound formation enthalpies for Eqs. (2)–(8). In this paper, we use for this purpose the pseudopotential momentum-space total-energy method[10] within the generalized gradient approximation of PW91 formulas,[11] and the ultrasoft pseudopotentials of Vanderbilt,[12] as implemented by the VASP code.[13] The defect systems are simulated by a single impurity in a 64-atom supercell, while the formation energies of other compounds are calculated from their primitive cells. We use the basis set energy cutoff of 292.16 eV with appropriate sampling k mesh following Monkhorst-Pack scheme for different unit cells.[14] The formation energies are well converged with the basis set and sampling k points. For example, the formation energy of Mn_{Al} in a 64 atom supercell changes by only 30 meV when the energy cutoff for the basis set is increased to 400 eV and the sampling k mesh is doubled to $4\times4\times4$.

Table I gives the calculated cohesive energies and the assumed structures used for element bulk Cu, Al, Ga, In, S, Se, Te, Mn, and the formation energies of their binary compounds and the formation energies of $CuAlS_2$, $CuGaS_2$, $CuInS_2$, $CuGaSe_2$, $CuGaTe_2$. The cohesive energies for Cu and Mn are corrected for spin-polarized atoms.[13] The calculated cohesive energies of S, Se, and Te are much larger than the experiment values, which may result from their highly open structures. Other calculations agree with our results. For example, the cohesive energy of Se obtained in Ref. 15 is 3.55 eV, differing from ours by only 0.04 eV.

Figure 1 shows the computed chemical potential domains for $CuAlS_2$, $CuGaS_2$, $CuInS_2$, $CuGaSe_2$, and $CuGaTe_2$. The total colored (red + yellow + green) areas are the allowed chemical-potential ranges for these chalcopyrites. In the white regions, the chalcopyrites are unstable with respect to competing phases shown in the figures. For example, in $CuAlS_2$ the top white area are excluded due to the precipitation of AlS and Al_2S_3, whereas the bottom white area are excluded due to the precipitation of CuS and Cu_2S. The yellow areas are regions where Mn-on-Cu is stable, whereas the green areas are regions where Mn-on-III are stable (cf. Sec. IV). Red areas denote formation of Mn chalcogenides (cf. Sec. III). We have neglected the effect of ordered defect structures[16] that further reduce the chemical potential domains. Comparing total colored (red+yellow+green) areas in Fig. 1 for $CuAlS_2$, $CuGaS_2$, and $CuInS_2$, we see their stability ranges are roughly comparable. The main competing compounds are M^{III}-S and M^{III}-Se binaries, rather than Cu-S and Cu-Se binaries. Although the formation energies are more negative along the series $CuInS_2 \rightarrow CuGaS_2 \rightarrow CuAlS_2$ (see the growing area of the large triangles in Fig. 1), competition from M^{III}-S binaries leads to exclusion of larger domains along this series (see the decreasing upper left white area). The stability ranges decrease along the series $CuGaS_2 \rightarrow CuGaSe_2 \rightarrow CuGaTe_2$.

III. EFFECT OF Mn ON CHALCOPYRITE STABILITY

When Mn is introduced into the chalcopyrite systems, the chemical domain may be further limited due to competing phases formed with Mn, e.g., MnS, MnSe, or MnTe. Therefore,

$$\Delta\mu_{\mathrm{Mn}} + \Delta\mu_{\mathrm{S}} \leqslant \Delta H_f(\mathrm{MnS}), \tag{9}$$

$$\Delta\mu_{\mathrm{Mn}} + \Delta\mu_{\mathrm{Se}} \leqslant \Delta H_f(\mathrm{MnSe}), \tag{10}$$

or

$$\Delta\mu_{\mathrm{Mn}} + \Delta\mu_{\mathrm{Te}} \leqslant \Delta H_f(\mathrm{MnTe}). \tag{11}$$

Since ΔH_f(MnS), ΔH_f(MnSe), or ΔH_f(MnTe) is a constant, the allowed $\Delta\mu_{\mathrm{S}}$, $\Delta\mu_{\mathrm{Se}}$, or $\Delta\mu_{\mathrm{Te}}$ values, and thus $\Delta\mu_{\mathrm{Cu}}$ and $\Delta\mu_{\mathrm{III}}$ values will strongly depend on $\Delta\mu_{\mathrm{Mn}}$. The red area in Fig. 1 denotes the region where chalcopyrite is unstable with respect to formation of MnS or MnSe, assuming $\Delta\mu_{\mathrm{Mn}} = -1.0$ eV. In $CuGaTe_2$ case, the red area (due to MnTe) will appear when $\Delta\mu_{\mathrm{Mn}}$ is greater than ΔH_f(MnTe), i.e., -0.61 eV. When $\Delta\mu_{\mathrm{Mn}}$ becomes less negative, i.e., Mn gets richer, $\Delta\mu_{\mathrm{S}}$, $\Delta\mu_{\mathrm{Se}}$, or $\Delta\mu_{\mathrm{Te}}$ is required to be lower to avoid the formation of MnS, MnSe, or MnTe, thus the red area will expand. Under extremely Mn rich conditions, i.e., $\Delta\mu_{\mathrm{Mn}} = 0$, the red areas will cover all the colored regions for $CuAlS_2$, $CuGaS_2$, $CuInS_2$, $CuGaSe_2$, and $CuGaTe_2$. This means that all of these chalcopyrite compounds may be unstable with respect to formation of MnS, MnSe, or MnTe when Mn is extremely rich.

The Al and Mn compounds, such as Al_6Mn, with relatively less negative formation energy, have no further restriction on chalcopyrite stability. For example, even under extremely Mn rich condition, the Al_6Mn compound create the restriction of $\Delta\mu_{\mathrm{Al}} \leqslant -0.22$ eV (cf. Table I), which is already a weaker condition than that imposed by AlS. Therefore, the limitation from Al and Mn compounds are not shown in Fig. 1. Clearly, MnS is excluding more domains than MnSe and MnTe for a given $\Delta\mu_{\mathrm{Mn}}$, since MnS has a more negative formation energy than MnSe and MnTe (cf. Table I).

TABLE II. Formation energy for Mn substituting the Cu or the III sites of chalcopyrites at different charge state. The Makov-Payne correction (Ref. 18) up to quadrupole term is included, using the experiment dielectric constants (Refs. 32,33).

System	Defect	ΔH (eV)
$CuAlS_2$	Mn_{Al}^{0}	$1.36+\Delta\mu_{\mathrm{Al}}-\Delta\mu_{\mathrm{Mn}}$
	Mn_{Al}^{+}	$1.47+\Delta\mu_{\mathrm{Al}}-\Delta\mu_{\mathrm{Mn}}+E_F$
	Mn_{Al}^{-}	$1.68+\Delta\mu_{\mathrm{Al}}-\Delta\mu_{\mathrm{Mn}}-E_F$
	Mn_{Cu}^{0}	$0.81+\Delta\mu_{\mathrm{Cu}}-\Delta\mu_{\mathrm{Mn}}$
	Mn_{Cu}^{+}	$-0.67+\Delta\mu_{\mathrm{Cu}}-\Delta\mu_{\mathrm{Mn}}+E_F$
	Mn_{Cu}^{-}	$3.24+\Delta\mu_{\mathrm{Cu}}-\Delta\mu_{\mathrm{Mn}}-E_F$
$CuGaS_2$	Mn_{Ga}^{0}	$0.22+\Delta\mu_{Ga}-\Delta\mu_{\mathrm{Mn}}$
	Mn_{Ga}^{+}	$0.31+\Delta\mu_{Ga}-\Delta\mu_{\mathrm{Mn}}+E_F$
	Mn_{Ga}^{-}	$0.57+\Delta\mu_{Ga}-\Delta\mu_{\mathrm{Mn}}-E_F$
	Mn_{Cu}^{0}	$0.61+\Delta\mu_{\mathrm{Cu}}-\Delta\mu_{\mathrm{Mn}}$
	Mn_{Cu}^{+}	$-0.52+\Delta\mu_{\mathrm{Cu}}-\Delta\mu_{\mathrm{Mn}}+E_F$
	Mn_{Cu}^{-}	$2.52+\Delta\mu_{\mathrm{Cu}}-\Delta\mu_{\mathrm{Mn}}-E_F$
$CuInS_2$	Mn_{In}^{0}	$-0.32+\Delta\mu_{In}-\Delta\mu_{\mathrm{Mn}}$
	Mn_{In}^{+}	$-0.15+\Delta\mu_{In}-\Delta\mu_{\mathrm{Mn}}+E_F$
	Mn_{In}^{-}	$-0.14+\Delta\mu_{In}-\Delta\mu_{\mathrm{Mn}}-E_F$
	Mn_{Cu}^{0}	$0.20+\Delta\mu_{\mathrm{Cu}}-\Delta\mu_{\mathrm{Mn}}$
	Mn_{Cu}^{+}	$-0.59+\Delta\mu_{\mathrm{Cu}}-\Delta\mu_{\mathrm{Mn}}+E_F$
	Mn_{Cu}^{-}	$1.37+\Delta\mu_{\mathrm{Cu}}-\Delta\mu_{\mathrm{Mn}}-E_F$
$CuGaSe_2$	Mn_{Ga}^{0}	$0.21+\Delta\mu_{Ga}-\Delta\mu_{\mathrm{Mn}}$
	Mn_{Ga}^{+}	$0.30+\Delta\mu_{Ga}-\Delta\mu_{\mathrm{Mn}}+E_F$
	Mn_{Ga}^{-}	$0.52+\Delta\mu_{Ga}-\Delta\mu_{\mathrm{Mn}}-E_F$
	Mn_{Cu}^{0}	$0.61+\Delta\mu_{\mathrm{Cu}}-\Delta\mu_{\mathrm{Mn}}$
	Mn_{Cu}^{+}	$-0.36+\Delta\mu_{\mathrm{Cu}}-\Delta\mu_{\mathrm{Mn}}+E_F$
	Mn_{Cu}^{-}	$2.09+\Delta\mu_{\mathrm{Cu}}-\Delta\mu_{\mathrm{Mn}}-E_F$
$CuGaTe_2$	Mn_{Ga}^{0}	$0.31+\Delta\mu_{Ga}-\Delta\mu_{\mathrm{Mn}}$
	Mn_{Ga}^{+}	$0.34+\Delta\mu_{Ga}-\Delta\mu_{\mathrm{Mn}}+E_F$
	Mn_{Ga}^{-}	$0.57+\Delta\mu_{Ga}-\Delta\mu_{\mathrm{Mn}}-E_F$
	Mn_{Cu}^{0}	$0.74+\Delta\mu_{\mathrm{Cu}}-\Delta\mu_{\mathrm{Mn}}$
	Mn_{Cu}^{+}	$0.09+\Delta\mu_{\mathrm{Cu}}-\Delta\mu_{\mathrm{Mn}}+E_F$
	Mn_{Cu}^{-}	$1.84+\Delta\mu_{\mathrm{Cu}}-\Delta\mu_{\mathrm{Mn}}-E_F$

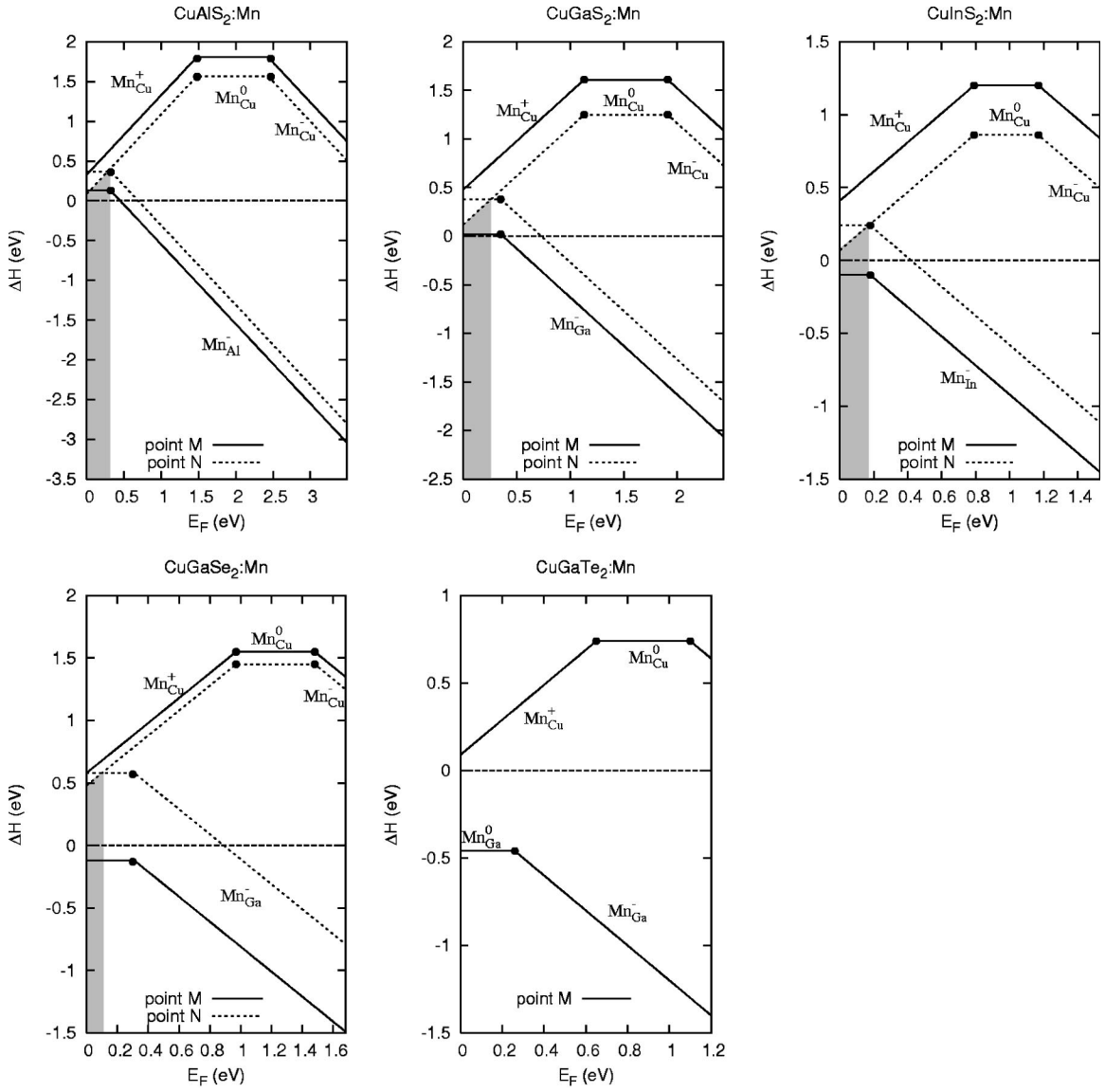

FIG. 2. The formation energy ΔH vs Fermi level for $CuAlS_2$:Mn, $CuGaS_2$:Mn, $CuInS_2$:Mn, $CuGaSe_2$:Mn, and $CuGaTe_2$:Mn with the chemical potentials at point *M* and *N* in Fig. 1. Mn prefers to III sites at point M, independent of E_F, while it prefers the Cu site at point N only in the shaded E_F ranges. For $CuGaTe_2$:Mn, Mn on Cu is unstable for all E_F values. Here chemical potential for Mn is set as -1.0 eV.

IV. SITE PREFERENCE OF Mn IN CHALCOPYRITES

Having calculated the chemical potential domains for $CuAlS_2$, $CuGaS_2$, $CuInS_2$, and $CuGaSe_2$ (Fig. 1), we next discuss the site preference of Mn in these chalcopyrites. The formation enthalpy for Mn substituting either the Cu or the III sites at different charge state are calculated using a single Mn atom in a 64 atom supercell according to[16,17]

$$\Delta H_f^{(\alpha,q)} = E(\alpha,q) - E(0) + \sum_\alpha n_\alpha(\Delta\mu_\alpha + \mu_\alpha^{\text{Solid}}) + q(E_{VBM} + E_F), \tag{12}$$

where $E(\alpha,q)$ and $E(0)$ are the total energy of the supercell with and without defect α. Here $(\Delta\mu_\alpha + \mu_\alpha^{\text{Solid}})$ is the absolute value of the chemical potential of atom α. Also n_α is the number of atoms for each defect; $n_\alpha = -1$ if an atom is added, while $n_\alpha = 1$ if an atom is removed. E_{VBM} represents the energy of the VBM of the defect-free system (which we take from the averaged eigenvalue of special *k* points) and E_F is the Fermi energy relative to the E_{VBM}. The atomic structure was fully relaxed in our calculation. The relaxation energy due to Mn substitution was 20–100 meV. The total energy of charged defects in a supercell calculation includes an error due to image charge interaction from periodic boundary condition. We therefore correct $E(\alpha,q)$ up to quadrupole term according to the Makov-Payne scheme.[18] The correction raised $E(\alpha,q)$ by 120 to 300 meV for both $q=1$ and $q=-1$ charge states.

The functional relations between the formation energy and chemical potentials and E_F at different charge states are listed in Table II. The site preference of Mn is determined by

the sign of $\Delta E \equiv \Delta H_f(\mathrm{Mn}_{\mathrm{Cu}}^q) - \Delta H_f(\mathrm{Mn}_{\mathrm{III}}^{q'})$, which is independent of $\Delta\mu_{\mathrm{Mn}}$, but depends on E_F. Although the Fermi level may be determined by charge neutrality condition, it is not easy to obtain unless all possible defects in these systems are known. If only the $\mathrm{Mn}_{\mathrm{Cu}}^q$ and $\mathrm{Mn}_{\mathrm{III}}^{q'}$ defects are considered, the Fermi level may be pinned at the transition level of $\mathrm{Mn}_{\mathrm{III}}(0/-)$ for most cases.[19] Experimentally, chalcopyrites tend to show *p*-type conductivity,[20,21] thus the Fermi level is close to VBM, although *n*-type conductivity could also be realized in some chalcopyrites.[22,23]

Figure 1 shows the possible Mn site preference at different $\Delta\mu_{\mathrm{Cu}}$, $\Delta\mu_{\mathrm{III}}$ regions, assuming[24,25] Fermi level at 0.1 eV above the VBM for all the systems. It indicates that Mn prefers the III site (green area) under Cu-rich and III-poor condition, whereas Mn prefers the Cu site (yellow area) under III-rich condition. Along the series $\mathrm{CuAlS_2} \rightarrow \mathrm{CuGaS_2} \rightarrow \mathrm{CuInS_2} \rightarrow \mathrm{CuGaSe_2} \rightarrow \mathrm{CuGaTe_2}$, the chemical potential domain for Cu site preference is reduced (cf. the shrinking yellow areas). At the same time, the domain for III site preference is increased (increasing green areas). As discussed above, the site preference depends on the sign of $\Delta H_f(\mathrm{Mn}_{\mathrm{Cu}}^q) - \Delta H_f(\mathrm{Mn}_{\mathrm{III}}^{q'})$. For E_F near the VBM, this difference consists mainly of two parts: $[E(\mathrm{Mn}_{\mathrm{Cu}},+) - E(\mathrm{Mn}_{\mathrm{III}},0)]$ and $(\Delta\mu_{\mathrm{Cu}} - \Delta\mu_{\mathrm{III}})$. In general, the first part increases rapidly along the $\mathrm{CuAlS_2} \rightarrow \mathrm{CuGaS_2} \rightarrow \mathrm{CuInS_2} \rightarrow \mathrm{CuGaSe_2} \rightarrow \mathrm{CuGaTe_2}$ chalcopyrite series (cf. Table II), while the higher limit of $(\Delta\mu_{\mathrm{Cu}} - \Delta\mu_{\mathrm{III}})$ increases slowly (cf. Fig. 1). Therefore, the Mn-on-III domain increases along this series.

To get a better description of the effect of E_F on the site preference, the dependence of the formation enthalpy on the Fermi level is shown in Fig. 2 for Mn in $\mathrm{CuAlS_2}$, $\mathrm{CuGaS_2}$, $\mathrm{CuInS_2}$, and $\mathrm{CuGaSe_2}$, at points *M* and *N* in the chemical potentials domains (cf. Fig. 1). Figure 2 shows the following.

(i) When E_F is located near the VBM, the $\mathrm{Mn}_{\mathrm{III}}$ is always charge neutral, while $\mathrm{Mn}_{\mathrm{Cu}}$ is at $+1$ charge state.

(ii) When E_F is close to the CBM, both $\mathrm{Mn}_{\mathrm{III}}$ and $\mathrm{Mn}_{\mathrm{Cu}}$ are in the negative charge state.

(iii) If the Fermi level moves toward the CBM, the area for $\mathrm{Mn}_{\mathrm{Cu}}$ preference in the $(\Delta\mu_{\mathrm{Cu}}, \Delta\mu_{\mathrm{III}})$ plane will be decreased. This is understandable since $\mathrm{Mn}_{\mathrm{Cu}}$ is energetically stable as a donor, whereas $\mathrm{Mn}_{\mathrm{III}}$ prefers to be an acceptor. Indeed, even for the point with the least negative (i.e., III-poor) $\Delta\mu_{\mathrm{III}}$ value in the colored area of Fig. 1, Mn prefers the III site when E_F passes the midgap toward the CBM. This means that the whole $\mathrm{Mn}_{\mathrm{Cu}}$ domain will be eliminated when E_F passes from the midgap to the CBM.

V. SUMMARY: TRENDS IN Mn SUBSTITUTION IN CHALCOPYRITES

(i) Pure chalcopyrites have a restricted range of chemical stability because under III-rich condition, it will precipitate $M^{\mathrm{III}}X^{\mathrm{VI}}$ compounds (e.g., AlS, GaS, InS, and $\mathrm{Al_2S_3}$, $\mathrm{Ga_2S_3}$, $\mathrm{In_2S_3}$), whereas under Cu-rich and III-poor conditions, it will precipitate $\mathrm{CuX}^{\mathrm{VI}}$ compounds.

(ii) Mn reduces the stability of chalcopyrites by excluding a domain where Mn*X* precipitates. This domain is larger for $X=S$ since the sulphide has more negative formation energy than for MnSe, MnTe. The Mn chemical potential strongly affects the stability of host: as Mn becomes maximally rich $(\Delta\mu_{\mathrm{Mn}}=0)$, the whole chalcopyrite domains are eliminated.

(iii) When the Fermi energy is near the VBM, $\mathrm{Mn}_{\mathrm{III}}$ is charge neutral and $\mathrm{Mn}_{\mathrm{Cu}}$ is positively charged. Both defects are in the negative charge state when E_F is close to the CBM.

(iv) The site preference of Mn on the Cu site is enhanced by III-rich chemical potential condition, whereas the preference of Mn on M^{III} site is enhanced by Cu-rich, III-poor conditions.

(v) The Fermi energy affects the Mn site preference: as E_F moves toward the CBM, the solubility of Mn on M^{III} increases, and that of $\mathrm{Mn}_{\mathrm{Cu}}$ decreases and disappears when E_F passes the midgap.

ACKNOWLEDGMENTS

Work supported by Office of Naval Research (ONR).

[1] H. Ohno, Science **281**, 951 (1998).
[2] S.A. Wolf, D.D. Awschalom, R.A. Buhrman, J.M. Daughton, S. von Molnr, M.L. Roukes, A.Y. Chtchelkanova, and D.M. Treger, Science **294**, 1488 (2001).
[3] A. Zunger, Solid State Phys. **39**, 275 (1986); H. Ohno, A. Shen, F. Matsukura, A. Oiwa, A. Endo, S. Katsumoto, and Y. Iye, Appl. Phys. Lett. **69**, 363 (1996); T. Dietl, Semicond. Sci. Technol. **17**, 377 (2002).
[4] G.A. Medvedkin, T. Ishibashi, T. Nishi, K. Hayata, Y. Hasegawa, and K. Sato, J. Mol. Biol. **39**, L949 (2000); S. Cho, S. Choi, G.-B. Cha, S.C. Hong, Y. Kim, Y.-J. Zhao, A.J. Freeman, J.B. Ketterson, B.J. Kim, Y.C. Kim, and B.-C. Cho, Phys. Rev. Lett. **88**, 257203 (2002); S. Choi, J. Choi, S.C. Hong, S. Cho, Y. Kim, and J.B. Ketterson, J. Korean Phys. Soc. **42**, S739 (2003).
[5] Y.-J. Zhao and A.J. Freeman, J. Magn. Magn. Mater. **246**, 145 (2002).
[6] P. Mahadevan and A. Zunger, Phys. Rev. Lett. **88**, 047205 (2002).
[7] T. Kamatani and H. Akai, Phase Transitions **76**, 401 (2003).
[8] S. Picozzi, Y.-J. Zhao, A.J. Freeman, and B. Delley, Phys. Rev. B **66**, 205206 (2002).
[9] T. Dietl, H. Ohno, and F. Matsukura, Phys. Rev. B **63**, 195205 (2001).
[10] J. Ihm, A. Zunger, and M.L. Cohen, J. Phys. C **12**, 4409 (1979).
[11] J.P. Perdew and Y. Wang, Phys. Rev. B **45**, 13 244 (1992).
[12] D. Vanderbilt, Phys. Rev. B **41**, 7892 (1990).
[13] G. Kresse and J. Furthmüller, Phys. Rev. B **54**, 11169 (1996); Computer code VASP (Institut für Materialphysik, Universität Wien, Wien, Austria).
[14] H.J. Monkhorst and J.D. Pack, Phys. Rev. B **13**, 5188 (1976).
[15] C. Kilic and A. Zunger, Phys. Rev. B **68**, 075201 (2003).
[16] S.B. Zhang, S.-H. Wei, A. Zunger, and H. Katayama-Yoshida, Phys. Rev. B **57**, 9642 (1998).

[17] S.B. Zhang, S.-H. Wei, and A. Zunger, Phys. Rev. Lett. **78**, 4059 (1997).
[18] G. Makov and M.C. Payne, Phys. Rev. B **51**, 4014 (1995).
[19] $Mn_{III}(0/-)$ means the Fermi energy at which $\Delta H(Mn_{III},q=0) = \Delta H(Mn_{III},q=-)$, see Fig. 2. When E_F is below $Mn_{III}(0/-)$, charges at Mn_{Cu}^{+} can not be balanced since Mn_{III} is at neutral state; when E_F is beyond $Mn_{III}(0/-)$ charges at Mn_{III}^{-} can not be neutralized since Mn_{III}^{-} has more population than Mn_{Cu}.
[20] M. Sugiyama, R. Nakai, and H.N.S.F. Chichibu, J. Appl. Phys. **92**, 7317 (2002).
[21] I. Aksenov and K. Sato, Jpn. J. Appl. Phys., Part 1 **31**, 2352 (1992).
[22] K.G. Lisunov, E. Arushanov, G.A. Thomas, E. Bucher, and J.H. Schön, Phys. Rev. Lett. **88**, 047205 (2002).
[23] B. Koscielniak-Mucha and A. Opanowicz, Phys. Status Solidi A **130**, K55 (1992).
[24] C. Kittel, *Introduction to Solid State Physics* 4th ed. (Wiley, New York 1971).
[25] P. Villars and L. Calvert, *Pearson's Handbook of Crystallographic Data for Intermetallic Phases* (American Society for Metals, Metals Park, OH, 1985), Vol. I.
[26] T. Asada and K. Terakura, Phys. Rev. B **47**, 15 992 (1993).
[27] Using the same structure of Ga_2Se_3, see Ref. 28.
[28] K. Ueno, M. Kawayama, Z.R. Dai, A. Koma, and F.S. Ohuchi, J. Cryst. Growth **207**, 69 (1999).
[29] S.-H. Wei and A. Zunger, Phys. Rev. B **48**, 6111 (1993).
[30] C. Wolverton, Acta Mater. **49**, 3129 (2001).
[31] D. Cahen and R. Noufi, J. Phys. Chem. Solids **52**, 947 (1991).
[32] M.I. Alonso, K. Wakita, J. Pascual, M. Garriga, and N. Yamamoto, Phys. Rev. B **63**, 075203 (2001).
[33] *LANDOLT-BÖRNSTEIN: Numerical Data and Functional Relationships in Science and Tecknology*, edited by K.-H. Hellwege, (Springer-Verlag, Berlin, 1980), Vol. III.